Polymer Testing 91 (2020) 106758

Contents lists available at ScienceDirect

Polymer Testing

journal homepage: http://www.elsevier.com/locate/polytest

Effect of L-Arginine treatment on the *in vitro* stability of electrospun aligned chitosan nanofiber mats

Paola Nitti [a,*], Nunzia Gallo [a], Barbara Palazzo [b,1], Alessandro Sannino [a], Alessandro Polini [c], Tiziano Verri [d], Amilcare Barca [d], Francesca Gervaso [a,c]

[a] Department of Engineering for Innovation, University of Salento, 73100, Lecce, Italy
[b] Ghimas S.p.A., c/o Dhitech S.c.a.r.l., 73100, Lecce, Italy
[c] CNR NANOTEC – Institute of Nanotechnology, 73100, Lecce, Italy
[d] Department of Biological and Environmental Sciences and Technologies, University of Salento, 73100, Lecce, Italy

ARTICLE INFO

Keywords:
Chitosan
Arginine
Crosslinking
Nanofiber alignment
Electrospinning
in vitro stability

ABSTRACT

Chitosan (Cs) mats obtained by electrospinning are potentially ideal scaffolds for tissue engineering. This technique allows obtaining nanometric fibrous structures with preferred orientation, which in turn enable cells to align themselves and produce extracellular matrix along desired orientations. In this study, we fabricated aligned Cs electrospun nanofiber mats and investigated the role of the amino acid L-Arginine (L-Arg) as stabilizing agent. Morphological, chemical, mechanical and biological characterizations were performed on untreated and L-Arg treated nanofibrous mats showing the role of L-Arg as biomimetic stabilizer. L-Arg acts as chemical stabilizer of nanofibrous mats, providing improved wettability behavior, mechanical properties and stability even after 60 days in aqueous medium in comparison to untreated mats. Moreover, preliminary biological tests demonstrated favorable cell-material interactions implying physiological responses in terms of viability and proliferation. The proposed L-Arg-treated Cs mats can be considered as potential scaffolds for highly oriented tissue patterning.

1. Introduction

In the field of tissue engineering, considerable attention has been increasingly given to the development of scaffolds using natural and biodegradable polymers [1–3]. Among them, chitosan (Cs), a cationic polysaccharide (N-deacetylated derivative of chitin), emerged as a promising biopolymer due to its biocompatibility, tailorable biodegradability, non-antigenicity, low cost, large availability, antimicrobial activity and wound healing potential [4–6]. Several studies reported the fabrication of Cs-based electrospun nanofibers as suitable mats for tissue engineering applications, because of their high surface area to volume ratio, interconnectivity, pore void volume, nanometer dimensions of the fibers that can be obtained and similarity to ECM structural components, typically in the 50–500 nm range [7–13]. Various polymers, including Cs, have been electrospun using rotating collectors, such as drums or disks, in order to obtain nanofiber mats with a preferred orientation [14,15], similarly to aligned collagen fibers present in natural extracellular matrix (ECM), which, in turn, enable cells to align themselves and produce matrix along desired orientation [16,17]. In order to successfully fabricate Cs nanofiber mats by electrospinning, highly viscous Cs solution can be combined with other polymers, such as poly (ethylene oxide) (PEO), to improve its processability [18].

As-produced Cs nanofiber mats in contact with water solutions swell and lose their fibrous structure [19]. Therefore, several crosslinking agents have been employed to tune their stability/degradability profile and provide them with suitable mechanical properties (in terms of stiffness, strength and toughness) *(i)* covalent crosslinkers (i.e. glutaraldehyde, glyoxal, ethylene glycol diglycidyl ether, genipin [20–22]): which have the disadvantage to take long reaction time and, in most cases, show cytotoxic effects [23], and *(ii)* ionic crosslinkers (i.e. glycerol phosphate, tripolyphosphate and tannic acid) which, at specific pH conditions, form networks through the electrostatic interactions of their

Abbreviations: Chitosan, Cs; Poly (ethylene oxide), PEO; L-arginine, L-Arg; Extra-cellular matrix, ECM.

* Corresponding author.
E-mail addresses: paola.nitti@unisalento.it (P. Nitti), nunzia.gallo@unisalento.it (N. Gallo), barbara.palazzo@enea.it (B. Palazzo), alessandro.sannino@unisalento.it (A. Sannino), alessandro.polini@nanotec.cnr.it (A. Polini), tiziano.verri@unisalento.it (T. Verri), amilcare.barca@unisalento.it (A. Barca), francesca.gervaso@nanotec.cnr.it (F. Gervaso).
[1] Current address: ENEA Division for Sustainable Materials, Research Centre of Brindisi, 72100, Italy.

https://doi.org/10.1016/j.polymertesting.2020.106758
Received 8 June 2020; Accepted 20 July 2020
Available online 14 August 2020

negatively charged groups with the positively charged groups of Cs chains [24–26]. Although ionic crosslinkers cannot be defined cytotoxic agents [27], they also may induce a slight cytotoxicity and a significant change in nanofiber morphology in view of modest increases in *vitro* stability and mechanical strength and stiffness [24,28,29]. However, among human biological tissues, those presenting highly fiber-oriented structures are primarily ligaments, tendons, muscles, i.e. all tissues in charge of sustaining important loads and showing, at the same time, a very low and rather slow regenerative potential [30]. Thus, durability and mechanical properties are core properties of an aligned nanofiber scaffold envisioned for highly oriented biological tissue regeneration.

With the aim of implementing a toxic chemical-free fabrication process of nanofiber scaffolds, the present study investigates the opportunity of using a biomolecule, i.e. L-Arginine (L-Arg) amino acid, as an ionic cross-linker for electrospun Cs nanofiber mats. L-Arg is a conditionally essential amino acid, involved as a precursor in many important biochemical pathways in cellular physiology (i.e. nitric oxide pathway involved in nerve regeneration) [31–33], and therefore an enhancer of some key cell processes, e.g. collagen synthesis, T-cell mediated responses, and also the release of pituitary hormones [34]. Recently, Antunes et al. [35] produced L-Arg grafted Cs and electrospun this modified polymer with the aim of increasing Cs mats antimicrobial activity. In our previously works, we proposed the use of L-Arg as a biomimetic stabilizing agent, employed in addition or substitution of the traditional polyanions to fine-tune microporous 3D scaffold properties [25,36]. Herein the L-Arg stabilizing role has been investigated for the first time on untreated electrospun Cs nanofiber mats. We first produced random and aligned nanofiber Cs mats by electrospinning, we treated them with L-Arg and, finally, investigated their morphology, wettability, *in vitro* stability, mechanical and biological properties.

2. Materials and methods

2.1. Materials

Low viscosity chitosan (Cs) from shrimp shells, poly (ethylene oxide) (PEO, average Mw 400 kDa), and common, high purity chemical reagents, such as L-Arginine (L-Arg), acetic acid (CH_3COOH, $\geq$ 99.7% wt), Phosphate buffered saline tablets (PBS), Tris (hydroxymethyl)aminomethane hydrochloride (TRIS HCl), sodium chloride (NaCl, $\geq$99% wt), sodium azide (NaN_3, $\geq$99.5% wt) together with all the other used materials and reagents, were purchased from Sigma-Aldrich (Milan, Italy), unless otherwise stated. All aqueous solutions were prepared with deionized and ultrapure water (18.2 MΩ/cm, obtained by a Milli-Q® Direct Water Purification System, Merck Millipore, Darmstadt, Germany).

2.2. Fabrication of aligned L-Arg-treated nanofiber Cs mats

Random and aligned Cs nanofiber mats were fabricated using several rotational speeds according to a previously optimized protocol [14]. Briefly, Cs and PEO powders were mixed at a 70/30 wt ratio and dissolved under magnetic stirring at room temperature by using a 90% v/v acetic acid water solution to obtain a homogeneous blend concentration of 4.5% w/v. PEO, a biocompatible and water-soluble polymer, was added to reduce the solution viscosity [37] and can be easily removed from electrospun fibers by washing [38]. The solution was processed via a commercial electrospinning apparatus (QCHV-M40, Linari Engineering s.r.l., Pisa, Italy) using a plastic syringe connected to a metallic needle (inner diameter: 0.8 mm). A solution flow rate of 0.02 mL/min, a voltage of 20–22 kV, and a needle-cylindrical drum collector (30 mm diameter, 120 mm length) at a distance of 13 cm were employed. The drum was rotated at 100 and 2000 rpm by a RT-Collector Web system (Linari Engineering s.r.l.) with a translation speed fixed at 10 mm/s, in order to obtain random-organized nanofiber Cs mats (hereafter called "random") and aligned nanofiber Cs mats (hereafter called "aligned"). Working temperature was about 25 °C. Cs/PEO mats were then recovered and dried under vacuum (P = 10 mbar) at 50 °C for 17 h prior to any further use. The as-produced random and aligned mats were subsequently immersed into aqueous L-Arg solution (200 mM, pH 11) for 24 h at 37 °C. Afterwards, the mats were washed with ultrapure water, until the washing solution reached pH 7, and then freeze dried for 17 h at 0 °C under vacuum (Coolsafe Freeze Dryer, Scanvac, Lillerød, Denmark).

2.3. Fiber morphology

Random and aligned, both untreated and L-Arg-treated mats were sputter coated with a 7 nm layer of gold and examined under scanning electron microscopy (SEM EVO® 40, Carl Zeiss AG, Oberkochen, Germany), in variable pressure mode and with an accelerating voltage of 20 kV. SEM micrographs were then analyzed by ImageJ 1.50c software (NIH, http://rsb.info.nih.gov/ij), in order to evaluate the average fiber diameter and size distribution in the electrospun mats (200 measurements for each acquired sample). The diameters are reported as average value ± standard deviation.

2.4. Mechanical properties

The mechanical properties of random and aligned, both untreated and L-Arg-treated mats were evaluated through a tensile test using a universal testing machine (ZwickiLine 1 kN, Zwick Roell, Kennesaw, GA, US), equipped with a 100 N load cell. Samples were hydrated in PBS (10 mM) for 2 h and tested in tension along the main nanofiber orientation. The average Young's modulus (E) was calculated as the slope of the linear elastic region of the stress-strain curve at low strain values (in the range 1–5%). Elongation at break ($\varepsilon_{\text{at break}}$) and tensile strength ($\sigma_{\text{at break}}$) were also measured. The results are expressed as average value ± standard deviation (n = 6).

2.5. Water contact angle measurements

The wettability of random and aligned, both untreated and L-Arg-treated mats was evaluated by measuring the static water contact angle (WCA) through sessile drop method (FTA1000 equipment Portsmouth, VA, US), placing a drop on the sample surface. At least 4 readings were performed for each specimen.

2.6. Stability test

The physical integrity of aligned untreated and Arg-treated mats in simulated physiological conditions (pH 7.4, temperature 37 °C) was evaluated by soaking the samples (30 mm × 10 mm) in 10 mL of TRIS-HCl buffer (50 mM, supplemented with NaCl 0.15 M and Sodium azide 0.01% wt, pH 7.4). At selected time points (3, 7, 15, 30 and 60 days), the samples (n = 6) were recovered, washed with distilled water, freeze-dried for 17 h and weighed. The percentage residual weight was then calculated using the following equation:

$$Residual\ Weight\ \% = \left(\frac{Wf}{Wi}\right) x\ 100 \quad (1)$$

where W_i is the initial weight of dried sample before soaking and W_f is the final weight after freeze-drying. Morphology of mats after incubation was qualitatively analyzed by SEM, while possible changes in mechanical properties were assessed by tensile test with the same protocol described above.

2.7. Cell viability assays (MTT)

NHI/3T3 mouse embryonic fibroblast (ATCC® CRL-1658™) were maintained in Dulbecco's modified Eagle medium (D-MEM)

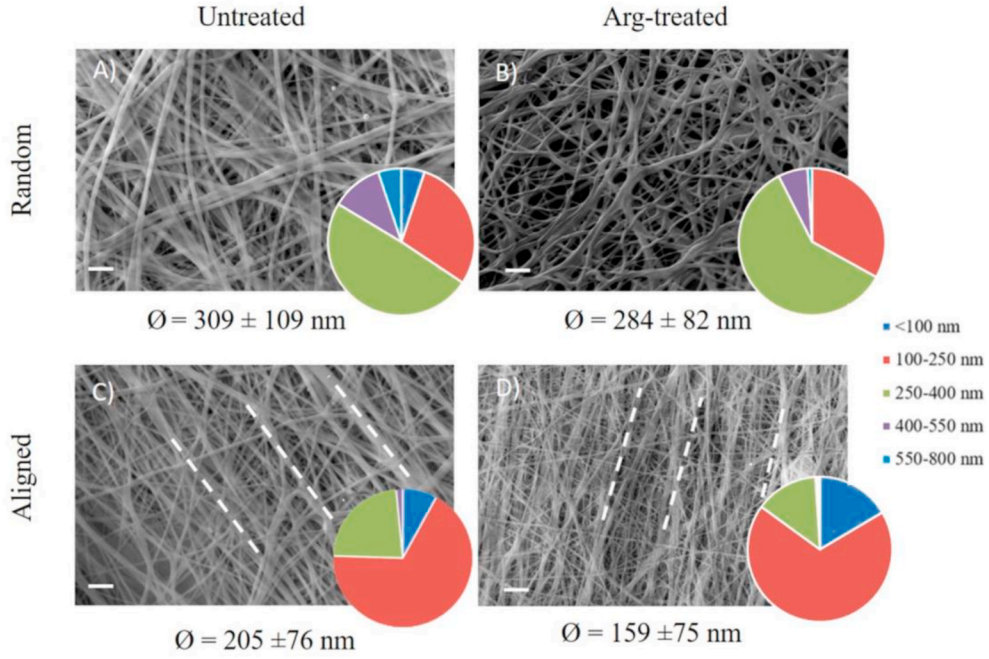

Fig. 1. SEM micrographs (scale bar: 2 μm) and fiber size distribution of random and aligned fibers, before (A and C) and after Arg-treatment (B and D).

supplemented with 10% (v/v) fetal bovine serum (FBS), 2 mM L-glutamine, and 100 μg/mL penicillin/streptomycin, in a humidified atmosphere (5% CO_2 in air) at 37 °C. Before cell seeding, aligned mats were cut into discs, sterilized by ethanol/D-PBS (Dulbecco's Phosphate Buffered Saline) solutions (EtOH 50% v/v 30 min, 70% 3 h, 50% 30 min) followed by D-PBS washing and ultraviolet (UV) irradiation for 2 h; then, mats were transferred into 24-well plates and incubated in cell culture medium. After 24 h, the medium was replaced with 200 μL of fresh medium containing 5×10^4 cells seeded on mats and into empty wells (as control growth surface). After 3 h, additional 100 μL of medium were added and cells were cultured for 24, 48 and 72 h. At each time point, samples were transferred to new sterile 24-well plates and incubated in fresh medium containing 50 μg/mL MTT (3-(4,5-dimethylthiazol-2-yl)-2,5-diphenyltetrazolium bromide) at 37 °C, for additional 4 h. Then, the medium was removed and the purple formazan crystals produced in cells by MTT metabolization were solubilized with acid isopropyl alcohol (0.04 M HCl). The absorbance of the solutions was measured (λ = 550 nm) by a Multiskan Fc Microplate Photometer (Thermo Fisher Scientific, Waltham, MA, US). For each sample, the absorbance arbitrary units were considered proportional to cell metabolic activity (viability). The procedure was also performed on blank mats (i.e. without cells) to assess interference by culture medium, and the absorbance values were normalized accordingly. All assays were repeated twice; six biological replicates for each sample category were tested.

2.8. Cell imaging

For cell imaging, standard protocols were performed for fluorescent staining of actin cytoskeleton and cellular nuclei, by using phalloidin-TRITC and DAPI, respectively. Before staining procedures, cells grown on aligned mats were fixed with 4% (w/v) paraformaldehyde (PFA) in D-PBS for 2 h (r.t.) followed by three D-PBS washings. Fixed samples were permeabilized by using 0.05% (w/v) Triton X-100 in D-PBS, with gentle orbital agitation for 10 min. Subsequently, samples were washed thrice in D-PBS, stained for 15 min with 0.1 mg/mL phalloidin-TRITC, and washed again thrice with D-PBS for 10 min (2 × 5 min). Then, nuclear staining with DAPI (1 μg/mL) was performed, followed by D-PBS washing for 10 min. Lastly, mats were directly reverse-mounted on microscope slides and observed by confocal microscopy. Images were acquired at 20X magnification, with a Zeiss LSM 710 confocal microscopy system, equipped with the ZEN 2009 software (LSM 710 suite). Cells on nanofibrous mats were also observed by SEM: after the fixation procedure, the mats were rinsed twice with D-PBS, dehydrated in scalar ethanol/water solutions (15% v/v, 25%, 50%, 70%, 90% and 100% ethanol, 10 min each), freeze-dried and coated with Au.

3. Results and discussion

Cs nanofiber mats have been proposed for tissue engineering applications, but their wide use is hindered by limited chemical stability and mechanical properties in aqueous solutions [8,39,40]. To achieve these purposes, it is necessary to stabilize the fiber mats against dissolution. In this study, the role of L-Arg as safe and biocompatible stabilizing agent of Cs-based nanofibrous mats was investigated.

3.1. Fiber morphology of stabilized Cs electrospun mats

Random and aligned Cs nanofiber mats were successfully produced by electrospinning and their morphology, before and after L-Arg treatment, was investigated by SEM (Fig. 1).

Nanofibers in random mats, both untreated and Arg-treated, do not present any preferential orientation (Fig. 1A-B). Arg-treated nanofibers appear slightly swollen and partially fused together forming a cross-linked net. The fiber distribution analysis revealed an average diameter of 309 ± 109 nm and 284 ± 82 nm for untreated and L-Arg-treated mats, respectively, with most of the fibers falling in the 250–400 nm range. Aligned mats showed a strong preferential nanofiber orientation (dashed lines in Fig. 1C-D) and a decrease in average fiber diameter: 205 ± 76 and 159 ± 75 nm for the untreated and L-Arg-treated mats, respectively. The distribution analysis highlighted that most of the fibers fall in the 50–500 nm range, similarly to ECM nanoarchitectures [8], in both untreated and Arg-treated mats. In comparison to random fibers, a decrease in fiber diameter and an overall increase in fiber distribution falling between 100 and 250 nm are noticeable in aligned mats, in accordance to previous reports [14,41]. The use of L-Arg as Cs stabilizer led to the fusion of neighboring fibers without, however, leading to an increase of average diameter in comparison to as-produced mats [42].

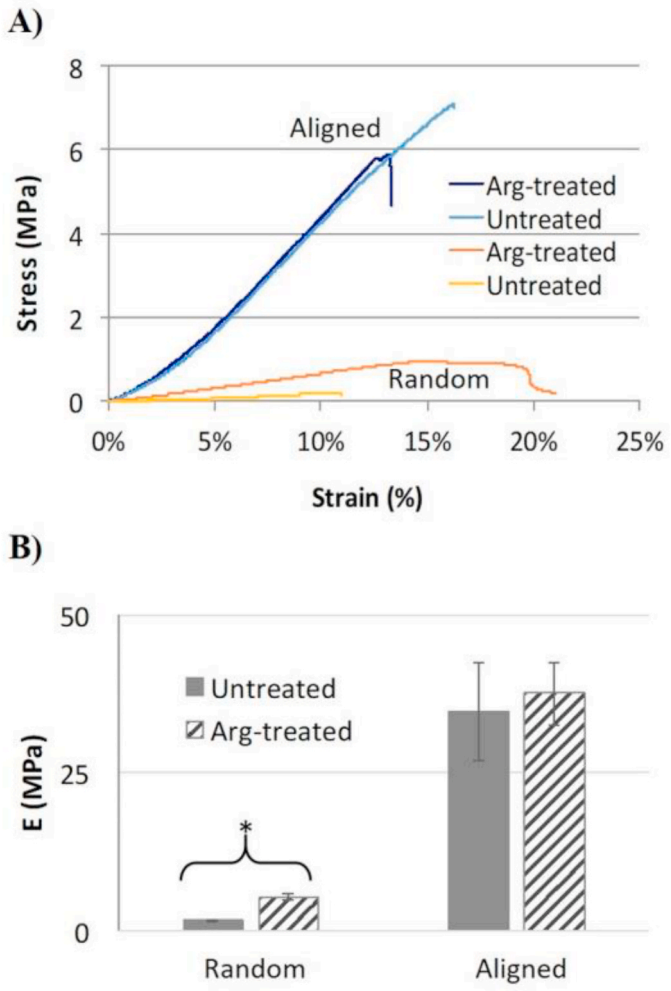

Fig. 2. A) Representative stress-strain curves and B) Young modulus (average values ± st.deviation, n = 6, *p < 0.05) of aligned and random samples, before and after Arg-treatment.

Moreover, the more branched and web-like morphology of stabilized fibers could be due to an increase in polymer chain-to-chain interactions [24]. The presence of L-Arg interacting with chitosan chains in the Arg-treated mats were confirmed by FT-IR spectroscopy (SI, Fig. S1).

3.2. Mechanical properties

Tensile tests were performed on random and aligned mats, before and after Arg-treatment (Fig. 2A). The stress-strain curves show a slightly non-linear elastic behavior, with a gradual increase in the stiffness corresponding to higher resistance to deformation, due to the higher intrinsic cohesive forces between fibers as long as the strain increases [21]. Additionally, the curves display a distinct maximum where the failure occurred during tension.

The aligned mats present significantly higher stiffness and tensile strength for both untreated and Arg-treated mats than random mats (Fig. 2A-B). This phenomenon is due to the increasing number of fibers aligned along the testing direction at high rotation speed. Tensile test also revealed that the effect of L-Arg is less evident for aligned fibers. Hence, as shown in the Young modulus histogram in Fig. 2B, the difference between the untreated and Arg-treated mat stiffness is significant for the random samples, while it is not significant for aligned ones. This result is likely related to the fact that at high rotation speeds, the fiber orientation effect is predominant and the L-Arg stabilizing effect is somehow hidden, while at low speed the fibers are not sufficiently aligned and the L-Arg stabilizing effect has stronger influence on the mechanical properties. A similar trend is shown by stress at break (σ at break) and strain at break (ε at break) that significantly increase after L-Arg treatment for random mats and are only slightly higher (untreated vs Arg-treated) for aligned mats (Table 1).

Table 1
Young's modulus (E), stress at break (σ at break), and strain at break (ε at break) of untreated and Arg-treated mats. Results are expressed as average value ± standard deviation.

Sample		E (MPa)	$\sigma_{\text{at break}}$ (MPa)	$\varepsilon_{\text{at break}}$ (%)
Random	Untreated	1.5 ± 0.3	0.2 ± 0.1	11 ± 2
	Arg-treated	5.3 ± 0.5	0.9 ± 0.3	17 ± 5
Aligned	Untreated	35 ± 8	6.5 ± 1.9	17 ± 3
	Arg-treated	38 ± 5	7.3 ± 2	18 ± 6

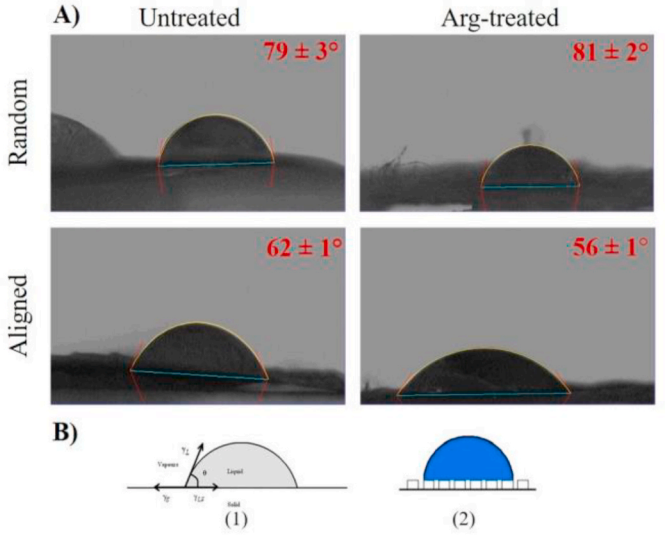

Fig. 3. A) Contact angle measurement of untreated and Arg-treated mats with different fiber orientation. B) Wetting behavior of solid substrates: Young (1) and Cassie regimes (2) [44].

3.3. Wettability measurements

The static WCA was evaluated to investigate the mat wettability. The random mats, untreated and L-Arg-treated, presented an average WCA of 79 ± 3° and 81 ± 2°, respectively, while aligned membranes, untreated and L-Arg-treated, of 62 ± 1° and 56 ± 1°, respectively (Fig. 3A). Random mats resulted more hydrophobic than aligned mats and the presence of L-Arg slightly increased the wettability of the aligned mats (smallest average WCA). Surface wettability is determined by the chemical composition and physical structure of the material [43]. Since the material is the same for the two different types of membranes, random and aligned, the wettability is likely influenced predominantly by morphological aspects, such as micro/nano-structure of the sample surface. Indeed, in a rough surface such as the one of the electrospun samples, the actual material surface in contact with the water droplet can be very different from the projected contact area of an ideal perfectly flat and rigid surface (Young regime, Fig. 3B1), thus strongly influencing the interfacial tension between the droplet and the sample and consequently the resulting contact angle. The random mats presented an increase of WCA with respect to aligned mats and this behavior could be in accordance with the Cassie regime (Fig. 3B2), that takes into account the presence of air pockets trapped under the liquid droplet [44].

The highly rough fibrous structure of the random mats likely traps

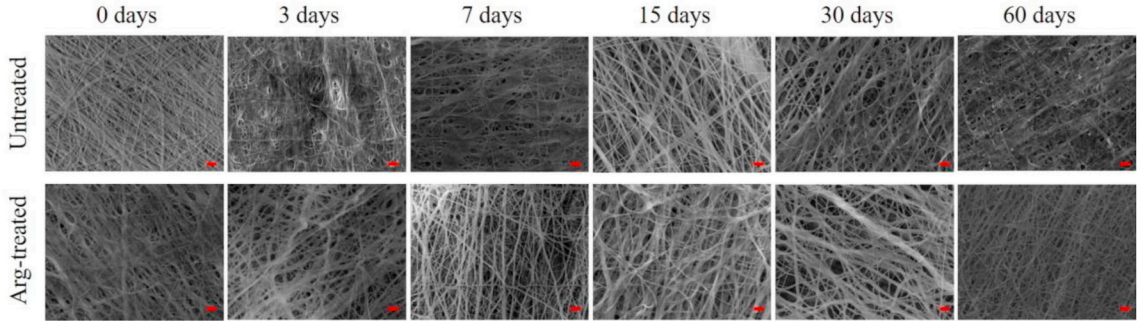

Fig. 4. SEM micrographs (scale bar: 2 μm) of untreated and Arg-treated mats after 0, 3, 7, 15, 30 and 60 days in TRIS-HCl pH 7.4 at 37 °C.

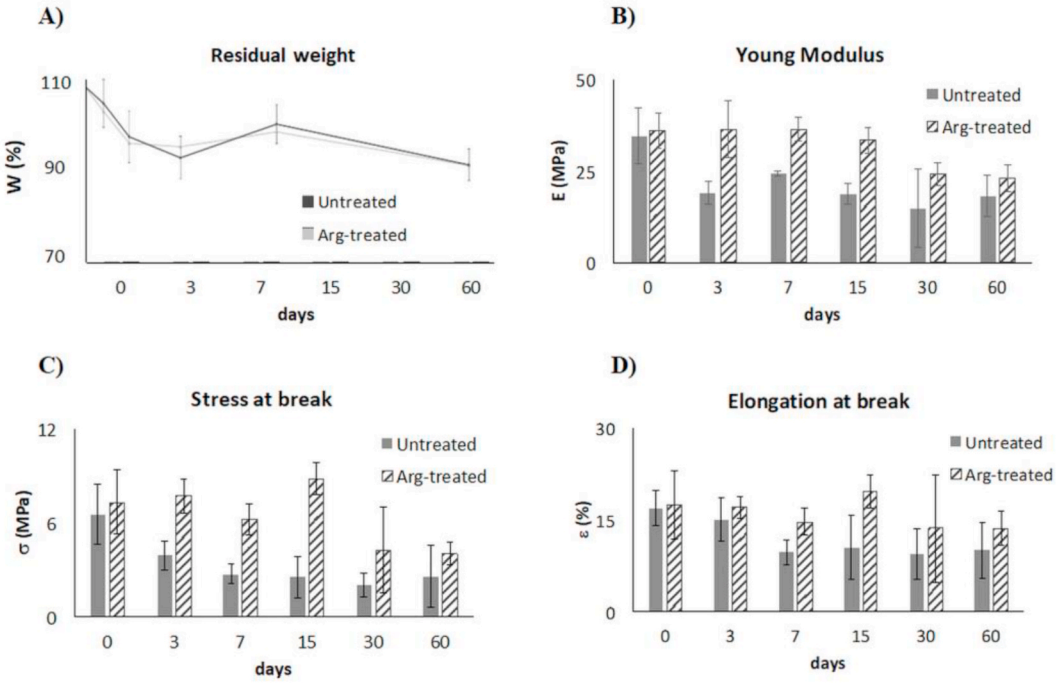

Fig. 5. Stability tests on untreated and Arg-treated aligned mats. A) Plot of residual weight (%) and results of tensile tests after 0, 3, 7, 15, 30 and 60 days of aging in TRIS-HCl pH 7.4 at 37 °C: B) Young modulus, C) stress at break, D) elongation at break.

some air pockets under the water droplet, thus giving rise to an increase of WCA with respect to the aligned mats in which the nanofibers are smaller, more ordered and closer each other. Surface wettability is one of the most important surface characteristics of biomedical materials, as cells better adhere, spread and grow on moderately hydrophilic substrates rather than on very hydrophobic or very hydrophilic ones [45]. The aligned Arg-treated mats presented the lowest WCA (i.e., highest wettability properties), suggesting that they might be a more cell-friendly biomaterial. The aligned mats (both Arg-treated and untreated) were selected for the following further investigation.

3.4. L-Arg effect on mats stability

To confirm the stabilizing effect of L-Arg and evaluate the stability of Cs nanofiber meshes in aqueous environment, untreated and Arg-treated aligned mats were immersed in TRIS-HCl buffer (pH 7.4) at 37 °C. At scheduled time, i.e. after 3, 7, 15, 30, and 60 days of immersion, stability performances of samples were checked through morphological, weight loss and mechanical evaluations.

All nanofibrous mats did not show considerable morphological changes in nanofibrous structure (Fig. 4). For untreated mats, an increase in the soaking time led to a partial fiber structure loss, as highlighted by the presence of fibers fused together [8,46]. On the contrary, Arg-treated mats preserved their integrity even up to 60 soaking days. Stability tests showed that both untreated and Arg-treated mats had a small weight loss after 3 days and, afterwards, remained substantially unchanged (Fig. 5A). After 60 days of incubation in aqueous medium, the remaining weight was 88% for both the mat typologies. Fig. 5B-D report the mechanical properties of the mats after each period of incubation. Beside time point 0, Arg-treated mats presented a Young modulus value (about 40 MPa) almost double than untreated mats (about 20 MPa) for each time point of aging in physiological solution and were stable up to 30 days showing a partial value reduction at day 30 and 60 (dropping to 20 MPa). In addition, stress and strain at break showed the same trend (Fig. 5C-D). These results highlight the stabilizing role of Arg.

The introduction of Arg slightly improved the tensile strength and elastic modulus. However, it is important to underline another effect of the Arg treatment, i.e. the removal of any residual acetic acid molecules. The acid protonation of the Cs amino residues is responsible for the polymer chains repulsions that in turns may cause the weakening of the untreated mats. L-Arg treatments likely reduced this effect and contemporarily stabilized mats through chains crosslinking. Therefore, the L-Arg treatment is responsible, from one side, for the neutralization

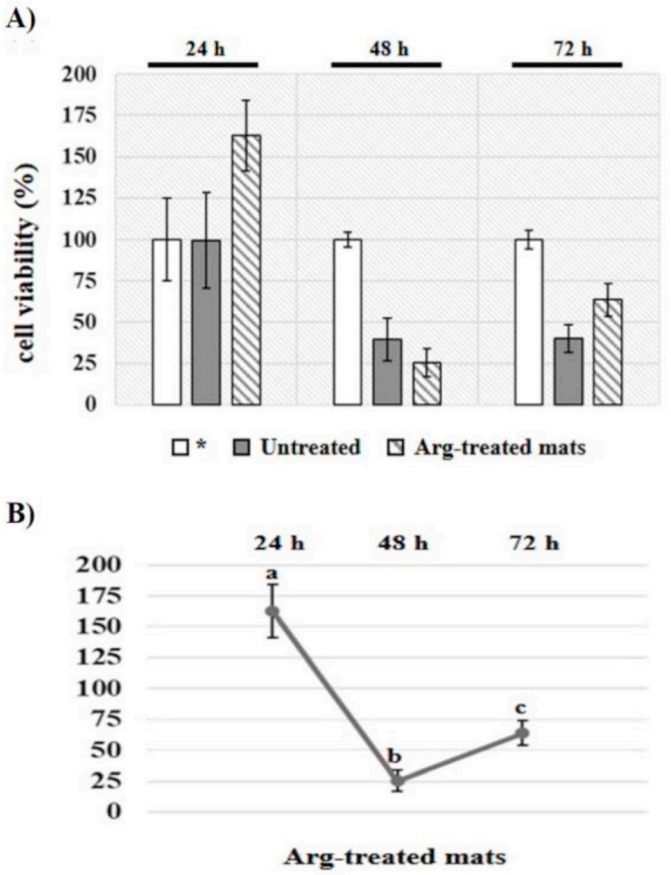

Fig. 6. (A) Viability of 3T3 murine fibroblasts on as-produced, Arg-treated mats and control culture plates (*), at 24, 48 and 72 h after seeding, assessed by MTT assays. At each time point, data are reported as % viability with respect to the control (100%); values are the average (±S.E.M.) of n = 6 independent replicates. (B) Detailed time course of cell viability on Arg-treated mats (statistical analysis: Student t-test; different letters indicate statistically different values; $p < 0.05$).

of acetic acid, with respect to the untreated mats, thus preventing the "destabilizing effect" deriving from the chains repulsion and a slightly acid-induced dissolution and, on the other side, for the stabilization of nanofiber mats through nanofiber crosslinking. In other words, the treatment preserves the nanofibrous architecture of mats (Fig. 4), but at the same time also positively influenced the mat mechanical properties (Fig. 5), that did not significantly change even after 2 months in aqueous solution.

Furthermore, foreseeing possible biomedical application of mats, we also investigated their thermal behaviour by differential scanning calorimetry (SI, Fig. S2) and concluded that the blend preparation, electrospinning process and L-Arg introduction did not affect significantly the thermal properties of their original components.

3.5. *Viability of murine fibroblast-like cells grown on mats and cell-material interactions in vitro*

Viability of cells cultured on untreated and Arg-treated mats was evaluated by MTT assays [8,46] in terms of metabolic activity.

Murine 3T3 fibroblasts were adopted being a long-established model for the tissue engineering studies of surfaces that mimic the ECM [47,48]. As summarized in Fig. 6A, Arg-treated mats exerted an early proliferative effect at 24 h *vs.* control cells seeded on the standard 2D growth surface (163% vs. 100% control). This effect might imply a metabolic boost elicited by immediate bioavailability of L-Arg for cells, thus enhancing their viability at short term.

Remarkably, this early onset was no more evident after 48 h, when a slowdown of proliferation was observed with respect to the control (25% *vs.* 100%), but at 72 h a recovery of cell metabolic activity was noticed (64% *vs.* 100%), with statistical significance (Fig. 6B). Interestingly, this behavior can be related to the improved stability at long (er) term promoted by L-Arg on the fibers, deserving further investigation. Contrarily, cells on untreated mats did not show either early (24 h) enhanced proliferation or later (72 h) recovery (Fig. 6A).

In parallel, the adhesion of viable 3T3 fibroblasts on mats was qualitatively analyzed by confocal microscopy (Fig. 7A).

At 24 h, although in both untreated and Arg-treated mats cells appeared as growing in clusters, on the Arg-treated mats more intense and diffused cytoskeletal actin staining was detected, suggesting the presence of a larger number of cells with advanced morphological differentiation. After 48 and 72 h, phalloidin-TRITC staining of actin cytoskeleton showed similar morpho-functional dynamics on both mats. Also, at 72 h it was possible to detect the recurrence of cell clusters proliferating following the general fiber orientation. When cells on untreated and Arg-linked mats were observed by SEM image acquisition, the presence of extended cellular filopodia aligned along the nanofibrous structures of the mat could be noticed, especially in Arg-treated samples (Fig. 7B).

Overall, the biological evidences indicate favorable cell-material interactions implying physiological responses in terms of viability and proliferation; also, L-Arg might have an interesting early boosting effect, which might be exploited as a modular factor to quantitatively improve the initial invasiveness of cells in the mat colonization process. Besides this, the fiber alignment might be exploited as a factor for enhancing the reproduction of an ordered structure resembling the ECM of native tissue districts.

4. Conclusions

The development of suitable biomimetic scaffolds that mimic the structure and biological characteristics of native ECM is a fundamental requirement for the treatment of injuries and diseases through a tissue engineering approach. In this study, electrospun aligned Cs nanofibrous mats were fabricated. These mats, being intended for biomedical applications, need to possess good chemical stability combined with good mechanical properties. To achieve these purposes, the Cs mats were treated with an amino acid, L-Arg, as a novel bioactive stabilizing agent. Arg-treated mats showed a fiber diameter fully comparable to the ECM architectures [49]. L-Arg improved the wettability and the architectural stability of nanofiber mats: specifically, we observed improved wettability and better mechanical properties for Arg-treated membranes in comparison to pristine mats. After 60 days in aqueous medium, untreated mats exhibited a partial loss of their original fiber structure, while the nanofiber morphology was preserved upon L-Arg treatment. These data are in agreement with the mechanical investigation, since Arg-treated post-stability mats presented higher elastic modulus than untreated post-stability mats. From these evidences, L-Arg demonstrated to be a good stabilizer for Cs nanofibers mats. We suggest that L-Arg treatment works as acid washing, being likely responsible for both the neutralization of residual acetic acid moieties with respect to the untreated mats and at the same time, stabilizes mats through interchain crosslinking. The cell-based tests using murine fibroblasts have further indicated the biomimicking suitability of the nanofibrous architectures to be exploited for soft tissue regeneration. Intriguingly, the introduction of L-Arg potentially shows to play a double role: as chemical stabilizer of nanofibrous mats providing improved mechanical properties and long-term stability on one hand and, on the other, as natural metabolic substrate for modulating cell-material interactions.

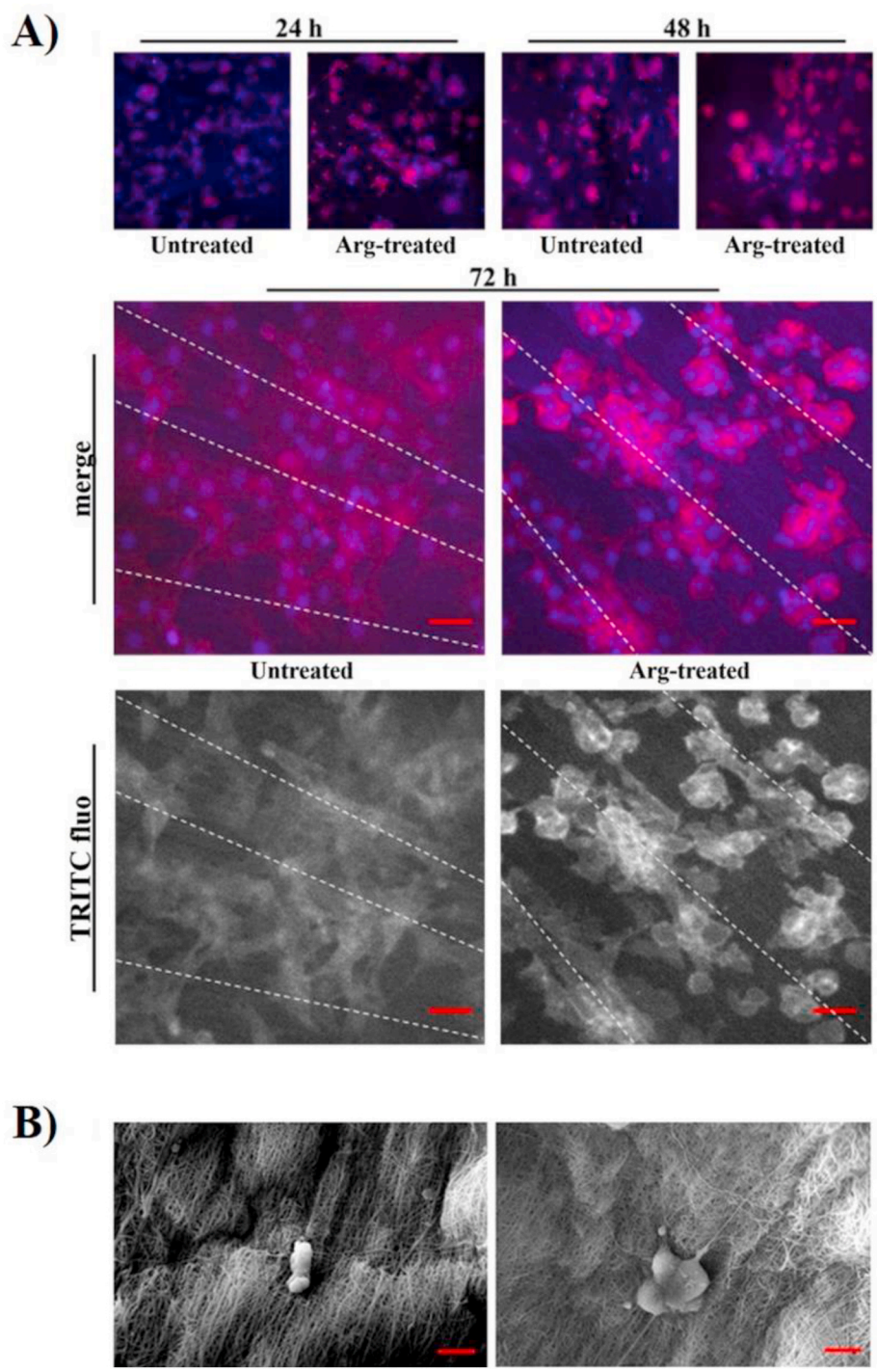

Fig. 7. 3T3 fibroblasts grown on untreated and Arg-treated mats. (A) Confocal microscopy merged images of phalloidin-TRITC (cytoskeletal actin filaments, red fluorescence signal) and DAPI (cell nuclei, blue fluorescence signal) staining after 24 h, 48 h and 72 h of culture (magnification: 10 × at 24–48 h; 20 × at 72 h). For the images of samples at 72 h, the splitted channel of the red fluorescence is also represented (TRITC fluo); white dotted lines are reported for tracing distribution of cells with respect to the alignment of mats fibers. (B) SEM micrographs of 3T3 cells grown on mats for 72 h [Scale bar: (a) 20 μm; (b) 10 μm]. (For interpretation of the references to colour in this figure legend, the reader is referred to the Web version of this article.)

Author contributions

The manuscript was written through contributions of all authors. All authors have given approval to the final version of the manuscript.

Funding sources

A. Polini and F. Gervaso acknowledge supports from the Progetto FISR – C.N.R. 'Tecnopolo di Nanotecnologia e Fotonica per la Medicina di Precisione', CUP B83B17000010001, and "Tecnopolo per la medicina di Precisione - Regione Puglia", CUP B84I18000540002.

Data availability statement

Data will be made available upon request to the corresponding author.

CRediT authorship contribution statement

Paola Nitti: Conceptualization, Methodology, Validation, Investigation, Writing - original draft. **Nunzia Gallo:** Validation, Investigation. **Barbara Palazzo:** Conceptualization, Writing - review & editing. **Alessandro Sannino:** Resources, Supervision. **Alessandro Polini:** Writing - review & editing. **Tiziano Verri:** Resources, Supervision.

Amilcare Barca: Investigation, Writing - review & editing. **Francesca Gervaso:** Conceptualization, Formal analysis, Writing - review & editing, Supervision.

Declaration of competing interest

The authors declare that they have no known competing financial interests or personal relationships that could have appeared to influence the work reported in this paper.

Acknowledgment

P. Nitti and N. Gallo gratefully acknowledge Dr. Sudipto Pal and Mr. Donato Cannoletta for the assistance with the contact angle measurements and the SEM imaging, respectively. Ms Laura Sercia is acknowledged for her help in hypothesizing the Arg-Cs interaction during her master thesis. P. Nitti and A. Barca thank Dr. G. Antonaci, and the 2HE-PONa3_00334 grant for the Zeiss LSM700 confocal microscopy and imaging of cells.

Appendix A. Supplementary data

Supplementary data to this article can be found online at https://doi.org/10.1016/j.polymertesting.2020.106758.

References

[1] R. Song, M. Murphy, C. Li, K. Ting, C. Soo, Z. Zheng, Current development of biodegradable polymeric materials for biomedical applications, Drug Des. Dev. Ther. 12 (2018) 3117–3145.
[2] H. Nosrati, S. Pourmotabed, E. Sharifi, A review on some natural biopolymers and their applications in angiogenesis and tissue engineering, Journal of Applied Biotechnology Reports 5 (2018) 81–91.
[3] S. Stratton, N.B. Shelke, K. Hoshino, S. Rudraiah, S.G. Kumbar, Bioactive polymeric scaffolds for tissue engineering, Bioact Mater 1 (2) (2016) 93–108.
[4] K. Kalantari, A.M. Afifi, H. Jahangirian, T.J. Webster, Biomedical applications of chitosan electrospun nanofibers as a green polymer - Review, Carbohydr. Polym. 207 (2019) 588–600.
[5] Y. Liu, M. Park, H. Shin, B. Pant, S.-J. Park, H.-Y. Kim, Preparation and characterization of chitosan-based nanofibers by ecofriendly electrospinning, Mater. Lett. 132 (2014) 23–26.
[6] X. Yan, Chitosan for tendon engineering and regeneration, in: J.A. Jennings, J. D. Bumgardner (Eds.), Chitosan Based Biomaterials, Tissue Engineering and Therapeutics, vol. 2, Woodhead Publishing, 2017, pp. 73–87.
[7] W.-J. Li, R. Tuli, C. Okafor, A. Derfoul, K.G. Danielson, D.J. Hall, R.S. Tuan, A three-dimensional nanofibrous scaffold for cartilage tissue engineering using human mesenchymal stem cells, Biomaterials 26 (6) (2005) 599–609.
[8] S.D. Sarkar, B.L. Farrugia, T.R. Dargaville, S. Dhara, Physico-chemical/biological properties of tripolyphosphate cross-linked chitosan based nanofibers, Mater Sci Eng C Mater Biol Appl 33 (3) (2013) 1446–1454.
[9] R. Jayakumar, M. Prabaharan, S.V. Nair, H. Tamura, Novel chitin and chitosan nanofibers in biomedical applications, Biotechnol. Adv. 28 (1) (2010) 142–150.
[10] A. Dodero, E. Brunengo, M. Alloisio, A. Sionkowska, S. Vicini, M. Castellano, Chitosan-based electrospun membranes: effects of solution viscosity, coagulant and crosslinker, Carbohydr. Polym. 235 (2020) 115976.
[11] P. Kianfar, A. Vitale, S. Dalle Vacche, R. Bongiovanni, Photo-crosslinking of chitosan/poly(ethylene oxide) electrospun nanofibers, Carbohydr. Polym. 217 (2019) 144–151.
[12] A. Rengifo, N. Stefanes, J. Toigo, C. Mendes, D. Argenta, M. Dotto, M.C. Santos-Silva, R. Nunes, T. Caon, A. Parize, E. Minatti, PEO-chitosan nanofibers containing carboxymethyl-hexanoyl chitosan/dodecyl sulfate nanoparticles loaded with pyrazoline for skin cancer treatment, Eur. Polym. J. 119 (2019) 335–343.
[13] M.B. Stie, M. Jones, H.O. Sørensen, J. Jacobsen, I.S. Chronakis, H.M. Nielsen, Acids 'generally recognized as safe' affect morphology and biocompatibility of electrospun chitosan/polyethylene oxide nanofibers, Carbohydr. Polym. 215 (2019) 253–262.
[14] P. Nitti, N. Gallo, L. Natta, F. Scalera, B. Palazzo, A. Sannino, F. Gervaso, Influence of nanofiber orientation on morphological and mechanical properties of electrospun chitosan mats, J Healthc Eng 2018 (2018) 3651480.
[15] L. Ricotti, A. Polini, G.G. Genchi, G. Ciofani, D. Iandolo, H. Vazão, V. Mattoli, L. Ferreira, A. Menciassi, D. Pisignano, Proliferation and skeletal myotube formation capability of C2C12 and H9c2 cells on isotropic and anisotropic electrospun nanofibrous PHB scaffolds, Biomed. Mater. 7 (3) (2012), 035010.
[16] G. Criscenti, A. Vasilevich, A. Longoni, C. De Maria, C.A. van Blitterswijk, R. Truckenmuller, G. Vozzi, J. De Boer, L. Moroni, 3D screening device for the evaluation of cell response to different electrospun microtopographies, Acta Biomater. 55 (2017) 310–322.
[17] A.F. Von Recum, T.G. Van Kooten, The influence of micro-topography on cellular response and the implications for silicone implants, J. Biomater. Sci. Polym. Ed. 7 (2) (1996) 181–198.
[18] R.R. Klossner, H.A. Queen, A.J. Coughlin, W.E. Krause, Correlation of chitosan's rheological properties and its ability to electrospin, Biomacromolecules 9 (10) (2008) 2947–2953.
[19] E. Mirzaei, R. Faridi-Majidi, M. Shokrgozar, F. Paskiabi, Genipin cross-linked electrospun chitosan-based nanofibrous mat as tissue engineering scaffold, Nanomedicine Journal 1 (3) (2014) 137–146.
[20] M.S. Austero, A.E. Donius, U.G. Wegst, C.L. Schauer, New crosslinkers for electrospun chitosan fibre mats. I. Chemical analysis, J. R. Soc. Interface 9 (75) (2012) 2551–2562.
[21] J.D. Schiffman, C.L. Schauer, Cross-linking chitosan nanofibers, Biomacromolecules 8 (2) (2007) 594–601.
[22] A. Aqil, V.T. Tchemtchoua, A. Colige, G. Atanasova, Y. Poumay, C. Jérôme, Preparation and characterizations of EGDE crosslinked chitosan electrospun membranes, Clin. Hemorheol. Microcirc. 60 (1) (2015) 39–50.
[23] V.A. Reyna-Urrutia, V. Mata-Haro, J.V. Cauich-Rodriguez, W.A. Herrera-Kao, J. M. Cervantes-Uc, Effect of two crosslinking methods on the physicochemical and biological properties of the collagen-chitosan scaffolds, Eur. Polym. J. 117 (2019) 424–433.
[24] M.A. Kiechel, L.T. Beringer, A.E. Donius, Y. Komiya, R. Habas, U.G. Wegst, C. L. Schauer, Osteoblast biocompatibility of premineralized, hexamethylene-1,6-diaminocarboxysulfonate crosslinked chitosan fibers, J. Biomed. Mater. Res. 103 (10) (2015) 3201–3211.
[25] D. Izzo, B. Palazzo, F. Scalera, F. Gullotta, V. lapesa, S. Scialla, A. Sannino, F. Gervaso, Chitosan scaffolds for cartilage regeneration: influence of different ionic crosslinkers on biomaterial properties, International Journal of Polymeric Materials and Polymeric Biomaterials 68 (15) (2019) 936–945.
[26] F.-L. Mi, H.-W. Sung, S.-S. Shyu, C.-C. Su, C.-K. Peng, Synthesis and characterization of biodegradable TPP/genipin co-crosslinked chitosan gel beads, Polymer 44 (21) (2003) 6521–6530.
[27] Z. Sang, J. Qian, J. Han, X. Deng, J. Shen, G. Li, Y. Xie, Comparison of three water-soluble polyphosphate tripolyphosphate, phytic acid, and sodium hexametaphosphate as crosslinking agents in chitosan nanoparticle formulation, Carbohydr. Polym. 230 (2020) 115577.
[28] F. Croisier, C. Jérôme, Chitosan-based biomaterials for tissue engineering, Eur. Polym. J. 49 (4) (2013) 780–792.
[29] C. Ceccaldi, E. Assaad, E. Hui, M. Buccionyte, A. Adoungotchodo, S. Lerouge, Optimization of injectable thermosensitive scaffolds with enhanced mechanical properties for cell therapy, Macromol. Biosci. 17 (6) (2017).
[30] J.T. Martin, A.H. Milby, K. Ikuta, S. Poudel, C.G. Pfeifer, D.M. Elliott, H.E. Smith, R. L. Mauck, A radiopaque electrospun scaffold for engineering fibrous musculoskeletal tissues: scaffold characterization and in vivo applications, Acta Biomater. 26 (2015) 97–104.
[31] J. Greene, J. Feugang, K. Pfeiffer, J. Stokes, S. Bowers, P. Ryan, L-arginine enhances cell proliferation and reduces apoptosis in human endometrial RL95-2 cells, Reproductive biology and endocrinology, RBE (Rev. Bras. Entomol.) 11 (2013) 15.
[32] K. Racké, M. Warnken, L-arginine metabolic pathways, Open Nitric Oxide J. 2 (2010) 9–19.
[33] V.B. Damodaran, D. Bhatnagar, H. Rubin, M.M. Reynolds, Chapter 6 - nitric oxide donors in nerve regeneration, in: A.B. Seabra (Ed.), Nitric Oxide Donors, Academic Press, 2017, pp. 141–168.
[34] H.P. Shi, S.M. Wang, G.X. Zhang, Y.J. Zhang, A. Barbul, Supplemental L-arginine enhances wound healing following trauma/hemorrhagic shock, Wound Repair Regen. 15 (1) (2007) 66–70.
[35] B.P. Antunes, A.F. Moreira, V.M. Gaspar, I.J. Correia, Chitosan/arginine–chitosan polymer blends for assembly of nanofibrous membranes for wound regeneration, Carbohydr. Polym. 130 (2015) 104–112.
[36] S. Scialla, A. Barca, B. Palazzo, U. D'Amora, T. Russo, A. Gloria, R. De Santis, T. Verri, A. Sannino, L. Ambrosio, F. Gervaso, Bioactive chitosan-based scaffolds with improved properties induced by dextran-grafted nano-maghemite and l-arginine amino acid, J. Biomed. Mater. Res. 107 (6) (2019) 1244–1252.
[37] N. Bhattarai, D. Edmondson, O. Veiseh, F.A. Matsen, M. Zhang, Electrospun chitosan-based nanofibers and their cellular compatibility, Biomaterials 26 (31) (2005) 6176–6184.
[38] N. Maeda, J. Miao, T.J. Simmons, J.S. Dordick, R.J. Linhardt, Composite polysaccharide fibers prepared by electrospinning and coating, Carbohydr. Polym. 102 (2014) 950–955.
[39] F. Ruini, C. Tonda-Turo, V. Chiono, G. Ciardelli, Chitosan membranes for tissue engineering: comparison of different crosslinkers, Biomed. Mater. 10 (2015), 065002.
[40] N. Grimmelsmann, T. Grothe, S. Homburg, A. Ehrmann, Electrospinning and stabilization of chitosan nanofiber mats, IOP Conf. Ser. Mater. Sci. Eng. 254 (2017), 102006.
[41] E. Medeiros, L. Mattoso, E. Ito, K. Gregorski, G. Robertson, R. Offeman, D. Wood, W. Orts, S. Imam, Electrospun nanofibers of poly(vinyl alcohol) reinforced with cellulose nanofibrils, J. Biobased Mater. Bioenergy 2 (2008) 231–242.
[42] H. Susanto, A. Muhamad Samsudin, M. Faz, Impact of post-treatment on the characteristics of electrospun poly (vinyl alcohol)/chitosan nanofibers, in: The 3rd International Conference on Advanced Materials Science and Technology (ICAMST 2015), 2015, 020087.
[43] A.D. Li, Z.Z. Sun, M. Zhou, X.X. Xu, J.Y. Ma, W. Zheng, H.M. Zhou, L. Li, Y. F. Zheng, Electrospun Chitosan-graft-PLGA nanofibres with significantly enhanced

hydrophilicity and improved mechanical property, Colloids Surf. B Biointerfaces 102 (2013) 674–681.
[44] D. Liviu, A. Popescu, I. Zgura, N. Preda, I. Mihailescu, Wettability of Nanostructured Surfaces (2015) 207–252.
[45] X. Zhu, W. Cui, X. Li, Y. Jin, Electrospun fibrous mats with high porosity as potential scaffolds for skin tissue engineering, Biomacromolecules 9 (7) (2008) 1795–1801.
[46] C. Tonda-Turo, F. Ruini, M. Ramella, F. Boccafoschi, P. Gentile, E. Gioffredi, G. Falvo D'Urso Labate, G. Ciardelli, Non-covalently crosslinked chitosan nanofibrous mats prepared by electrospinning as substrates for soft tissue regeneration, Carbohydr. Polym. 162 (2017) 82–92.
[47] S.R. Peyton, C.M. Ghajar, C.B. Khatiwala, A.J. Putnam, The emergence of ECM mechanics and cytoskeletal tension as important regulators of cell function, Cell Biochem. Biophys. 47 (2) (2007) 300–320.
[48] T. Kutlusoy, B. Oktay, N.K. Apohan, M. Süleymanoğlu, S.E. Kuruca, Chitosan-co-Hyaluronic acid porous cryogels and their application in tissue engineering, Int. J. Biol. Macromol. 103 (2017) 366–378.
[49] H.K. Noh, S.W. Lee, J.-M. Kim, J.-E. Oh, K.-H. Kim, C.-P. Chung, S.-C. Choi, W. H. Park, B.-M. Min, Electrospinning of chitin nanofibers: degradation behavior and cellular response to normal human keratinocytes and fibroblasts, Biomaterials 27 (21) (2006) 3934–3944.